An EBSD analysis of Fe-36%Ni alloy processed by HPT at ambient and a warm temperature

Kamel Tirsatine[a], Hiba Azzeddine[a,b,*], Yi Huang[c], Thierry Baudin[d], Anne-Laure Helbert[d], François Brisset[d], Djamel Bradai[a], Terence G. Langdon[c]

[a] Faculty of Physics, University of Sciences and Technology Houari Boumediene, Bab- Ezzouar, BP32, El Alia, Algiers, Algeria
[b] Faculty of Sciences, University of M'Sila, Algeria
[c] Materials Research Group, Faculty of Engineering and the Environment, University of Southampton, Southampton SO17 1BJ, UK
[d] ICMMO, SP2M, Univ. Paris-Sud, Université Paris-Saclay, UMR CNRS 8182, 91405 Orsay Cedex, France

Abstract

Electron backscatter diffraction (EBSD) was used to evaluate the evolution of microstructure and texture in an Fe-36%Ni (wt. %) alloy after processing by high-pressure torsion (HPT) up to 10 turns at ambient temperature and 250 °C. HPT processing led to a strong microstructural refinement with average grain sizes of ~ 0.30 and ~ 0.24 μm at ambient temperature and 250 °C, respectively. The high-angle grain boundary fraction was slightly higher after processing at 250 °C and gradually increased with increasing numbers of HPT turns to saturate after 5 turns. The crystallographic texture after HPT processing at ambient temperature was characterized by typical A and B fibers of a simple shear FCC texture with domination of the *B* component. By contrast, the *A*, *B* and *C* components developed during HPT processing at 250 °C with *C* as the dominant texture component. The microhardness values for both HPT deformation conditions were very similar with a continuous increase with increasing HPT turns and almost saturation after 5 HPT turns. The grain size dependence of the microhardness followed the Hall-Petch relationship. The explanation for the microstructure, texture and microhardness difference was attributed to a dynamic recovery process that operates during processing at 250 °C.

Keywords: High-Pressure Torsion; Invar alloy; Microstructure; Texture; Ultrafine-Grained Metals.

* Corresponding author: azehibou@yahoo.fr, Tel: +213 6 59 07 29 02

1. Introduction

Ultrafine grained (UFG) materials produced by severe plastic deformation (SPD), using procedures such as equal-channel angular pressing (ECAP) [1], accumulative roll bonding (ARB) [2] and high-pressure torsion (HPT) [3], have attracted much attention during the last decade due to the possibility of enhancing the properties of materials and producing multifunctional commercial alloys and composites [4–7].

HPT processing is one of the best techniques in term of the efficiency in grain size reduction, the formation of regularly shaped nano-grains and the potential for achieving a high fraction of high-angle grain boundaries [7, 8]. However, this type of SPD processing is generally suitable only for the fabrication of small pieces that may be of use in dental implants or micro-electro-mechanical systems (MEMS) [9]. Until now, the ARB process is the most appropriate for fabrication of sheet-shaped materials and this has a major advantage for industrial production. Furthermore, the evolution of the microstructure and texture of severely deformed Fe-36%Ni (wt. %) alloy by ARB processing was largely described in several earlier reports [10–12]. Nevertheless, the results showed that ARB processing led to the development of elongated ultrafine grains lying parallel to the rolling direction and with a texture gradient represented by a strong Copper/Dillamore component near the mid-thickness and a C component at the surface of the sheets [10].

Initially, HPT processing was used with Fe-Ni alloys in order to produce rare-metal-free magnetic material with nanoscale resolution by improving their magnetic domains [13–16]. It is well known that HPT processing is accompanied by a strong evolution of texture and microstructure but to date there has been no systematic study of the textural, microstructural and strength evolution of Fe-Ni alloys after processing by HPT at different temperatures. Accordingly, the aim of this research was to investigate the microstructure and texture evolution of an Fe-36%Ni (wt. %) alloy processed by HPT at the two temperatures of room temperature and 250 °C through up to a maximum of 10 turns.

2. Materials and methods

The Fe-36%Ni (wt. %) alloy was provided by APERAM Alloys Imphy society, France, and a detailed description of the initial microstructure and texture was given in an earlier report [10]. For HPT processing, disks were sliced from the as received material with thicknesses of ~ 0.9 mm. These disks were processed at ambient temperature and 250°C through totals of 1/2, 1, 5 and 10 turns using an imposed pressure of 6.0 GPa, a rotational speed of 1 rpm and quasi-

constrained conditions, where there is a small outflow of material around the periphery of the disk during the straining operation [17].

The microstructure and microtexture were characterized using a scanning electron microscope FEG-SEM SUPRA 55 VP operating at 20 kV with TSL Orientation Imaging Microscopy, OIM^{TM} software. EBSD maps were collected at the mid-radius of each disk on 100 × 100 μm zones perpendicular to the HPT rotation axis using a step size of 50 nm. The grain size data were obtained using a grain tolerance angle of 5° and the minimum grain size was chosen as 5 pixels. All datum points with a confidence index (CI) lower than 0.05 were excluded from the analysis where CI quantifies the reliability of the indexed pattern. Quantitative texture analysis was carried out by calculating the Orientation Distribution Function (ODF) using MTex software [18].

Vickers microhardness measurements were conducted in the center of the disks using a ZwickRoell ZHV10 tester. A load of 100 g and a dwell time of 10 s were used for all measurements.

3. Results

Figs. 1 and 2 present the inverse pole figure (IPF) maps with crystallographic directions parallel to the HPT rotation axis and these maps depict the microstructures of the Fe-36%Ni alloy after HPT processing for 1/2 to 10 turns at ambient temperature and 250 °C, respectively. The initial microstructures were composed of equiaxed grains with a mean grain size of ~8.2 μm [10]. A significant orientation spread within the individual grains due to the development of a substructure can be observed in the IPF maps for both temperature conditions after 1/2 turn. Moreover, the IPF maps of 1/2 HPT turn exhibits a bimodal grain size distribution with a large fraction of large grains mixed with several regions containing significantly fine equiaxed grains. However, the grain structure became more uniform with increasing numbers of HPT turns for both processing temperatures.

The evolution of the mean grain size and the fraction of high-angle grain boundaries (HAGB) as a function of the numbers of HPT turns at room temperature and 250 °C, respectively, are shown in Fig. 3. The grains underwent a strong refinement upon straining, especially during the first turn, and their size saturated at ~ 0.30 and ~ 0.24 μm after 5 HPT turns at room temperature and 250 °C respectively. The fraction of HAGB presented in Fig. 3 increases rapidly with increasing HPT turns to reach a saturation value around ~ 58.1 and ~ 66.5 % after 5 HPT turns at ambient temperature and 250 °C, respectively.

Fig. 4 shows the texture evolution of the Fe-36%Ni alloy after HPT processing for 1/2 to 10 turns at ambient temperature and 250 °C, respectively. The ideal HPT orientations for FCC materials are presented in the ODF figure of 1/2 turn at 250 °C and their characteristics are summarized in Table 1. As reported earlier, the initial texture was typical of annealed FCC materials where the Cube {001}<100> component dominated [10]. After HPT processing at ambient temperature to 1/2 turn, the *C*, $\overline{B}$ and $\overline{A}$ developed and with increasing deformation the A_1^* and *B* components appeared allowing the formation of A and B texture fibers. The A fiber is known to contain the *A*, $\overline{A}$, A_1^* and A_2^* ideal components, while the B fiber contains *A*, $\overline{A}$, *B*, $\overline{B}$ and *C* [19].

The volume fractions of different shear components plotted against the number of HPT turns for both temperature conditions, with an orientation tolerance of 15°, are shown in Fig. 5. It is apparent from Fig. 4 that the texture intensity does not change (~ 4 mrd) during the HPT processing but reinforcements around the *B* component are apparent after 5 HPT turns at ambient temperature. By contrast, the HPT processing at 250 °C led to the appearance of all shear texture components after only 1/2 turn except for the A_2^* component which, incidentally, was not observed after processing at ambient temperature. Moreover, the texture intensity after HPT processing at 250 °C decreases with increasing numbers of HPT turns and this leads to the disappearance of the A and B fibers. As can be demonstrated from Fig. 4, the remaining texture components after 5 HPT turns were only *A*, *B* and *C* and the *C* component exhibited a slight reinforcement (~ 4 mrd) after 10 HPT turns. Such reinforcement arises because the grains with A^* and *A* orientations may easily rotate to the vicinity of *C* and *B* orientations [20].

The evolution of microharness in the Fe-36Ni alloy after HPT processing at 25 and 250 °C is presented in Fig. 6. It is readily apparent that the microhardness values of the HPT sample processed at 250 °C are very close to those after processing at 25 °C. Moreover, the microharness increases significantly from the initial state (~ 177 Hv) to 1/2 HPT turn (~ 256 Hv). This strengthening is continuous with further torsional straining but tends to saturate after 5 HPT turns (~ 387 Hv). A similar microhardness evolution was reported in an Fe-50%Ni (at. %) alloy processed by HPT at room temperature for up 10 turns [16].

4. Discussion

The microstructure in terms of grains size and HAGB and mechanical properties evolution presented in this study demonstrate that HPT processing at 25 and 250 °C leads to an overall

saturation after 10 turns. The significance of these results are examined in the following sections.

4.1. Microstructure evolution after HPT processing

The microstructure of both HPT processing conditions exhibit significant grain refinement as is apparent from Figs 1–3. For comparison, different grain size values of ~ 0.20 μm were reported in commercial Cu–2.5%Ni–0.6%Si (wt.%) [7] and Al–0.6% Mg–0.4% Si (wt.%) [21] alloys after processing by HPT at ambient temperature up to 10 turns. Furthermore, the grain size is generally expected to vary essentially linearly with the temperature of processing [22, 23]. Contrary to this assumption, the present results show that the grain size is slightly lower after HPT processing at 250 °C than at ambient temperature. It is important to note that a similar evolution was reported earlier for a Mg-Al-Zn alloy after HPT processing at 23 and 100 °C [24].

The correlation between the sub-grain structure and the strength of structural materials is well known [25]. However, it has been observed that the shear strength of Cu does not decrease significantly with increasing processing temperature from room temperature to 150 °C [26]. Consequently, it was suggested that if the processing temperature was below the recrystallization range the shearing strength should be relatively insensitive to temperature changes [26]. Thus, a significant grain refinement from an initial grain size of ~ 800 μm to ~ 0.12 μm was reported in Fe-50%Ni (at. %) alloy processed by HPT at ambient temperature [16]. This grain size was retained at ~ 0.12 μm during subsequent annealing at 310 °C for 40 days. There are also published results on the kinetics of recrystallization of the Fe-36%Ni alloy after conventional cold rolling and severe plastic deformation (hot ARB) and subsequent annealing at 600 °C [27, 28]. The recrystallization of the Fe-36%Ni alloy after cold rolling and hot ARB was shown to occur after as late as several minutes or more than five minutes of annealing. Furthermore, the recrystallization was not fully achieved even after 1 hour annealing. In the present work, the material was HPT processed at 250 °C which is far less than the effective temperature for recrystallization and/or grain growth. Therefore, it is concluded that the temperature at 250 °C for HPT processing has a relatively weak effect on the microstructural evolution of the Fe-36% alloy.

The value of HAGB in Fig. 3 is very close to the value observed (~ 68 %) for a Cu-2.5%Ni-0.6%Si (wt. %) alloy processed by HPT [7] and also to the value reported (~ 60 %) for a Fe-36%Ni (wt. %) alloy processed by ARB [10]. It is well known that during the early stages of processing in FCC materials the microstructure contains a large fraction of LAGB and these boundaries transform into HAGB with increasing strain [29]. It was reported that the fraction

of HAGB increases more rapidly at low strain and then saturates (~ 85 %) at large strain in an Fe-32%Ni (wt. %) alloy deformed by multi-axial forging after a cumulative strain of ε ≈ 10.5 [30]. The HAGB fraction was slightly higher after processing at 250 °C and this is because the rate of dislocation and low-angle boundary annihilation is higher during processing at 250 °C than at ambient temperature. Nevertheless, it is clear from Fig. 3 that there remains a large fraction of LAGB in samples even after processing through 10 turns (~42.1 and ~33.5 % at ambient temperature and 250 °C, respectively). This is attributed to the continuous introduction of dislocations during the accumulative processing by HPT [7, 31].

4.2. Texture evolution after HPT processing

For a better comparison between the textures after ambient temperature and 250 °C, it is interesting to estimate the texture strength index which can be calculated from the equation [32]:

$$I = \frac{1}{8\pi^2}\int_G f^2(g)dg \quad (1)$$

where *f(g)* is the ODF values and *G* is the Euler space.

A material with a random texture has an *I* value equal to unity while a single component texture should have an infinite *I* [32]. The evolution of texture index of the Fe-36%Ni processed by HPT at ambient temperature and 250 °C is represented in Fig. 7. The texture index of the alloy processed by HPT at ambient temperature appears to increase slightly with increasing numbers of HPT turns to reach a value of ~1.5 after 10 turns. However, it is clearly seen that HPT processing at 250 °C results in a continuous decrease of the texture index to a minimum value around ~1.2 after 5 turns. Such quantitative results demonstrate a net tendency towards texture weakening and randomization upon increasing the numbers of HPT turns for the sample processed at 250 °C.

It is to be noted that the texture intensities for both processing conditions are very weak compared to those measured in the same alloy processed by ARB and cross accumulative roll bonding (CARB) at 550 °C [10, 11]. In fact, the texture evolution at the surface of a Fe-36%Ni sample processed by ARB [10] and CARB [11] exhibited a strong continuous strengthening of the *C* component with increasing strain. Such differences are attributed to the nature of the processing and the development of increasing grain refinement with increasing strain.

In Al-based alloys processed by HPT at room temperature, the texture at low strain was shown to be dominated by orientations mainly belonging to the A fiber, whereas with increasing strain level the *C* component becomes stronger and dominates so that the texture weakens and becomes randomized at high strain [33, 34]. In a copper-based alloy the texture after HPT at room temperature was characterized by the development of typical shear components of FCC metals in the initial stage of deformation. With increasing strain, the texture exhibited a reinforcement and saturation around a single A_1* component and a disappearance of the C component [7]. A close examination of the results for all the above alloys shows that neither the components nor their intensities were comparable with the data obtained in the present investigation. These differences between Fe-Ni, Al-Mg-Si and Cu-Ni-Si alloys processed by HPT and/or ARB are probably due to the differences in their stacking fault energy, γ_{SFE}, which directly determines the restoration behavior (recovery and recrystallization) of the deformed alloys. The reduced (or normalized) stacking fault energy is defined as $\gamma_{RSFE} = \gamma_{SFE}/Gb$ where *G* is the shear modulus and *b* is the length of the Burgers vector. Thus, it is has been reported that the ratio γ_{RSFE} (Al): γ_{RSFE} (FeNi): γ_{RSFE} (Cu) is equal to 7:3:1 [27].

Thus, in practice the Fe–36%Ni alloy has an intermediate stacking fault energy lying between the Cu-based and Al-based alloys and therefore, the deformation and recrystallization texture should be similar to that of Al or Cu. Nevertheless, the results show this alloy recovers only very little during cold deformation and it is well established from earlier analyses of hardness data [35] data that this is due specifically to its higher melting temperature. The rate of recovery should also drastically change owing to the nature of the severe plastic deformation processing. Thus, a plausible explanation for the development of all shear components after HPT processing at ambient temperature and a dominant *C* component at 250 °C lies in the dynamic recovery that operates at the higher temperature of 250 °C.

4.3. Microhardeness evolution after HPT processing

The evolution of microhardness as shown in Fig. 6 can be partitioned into two regions. The first region is a significant increase in hardness which is attributed to the accumulation of dislocation and the decrease of grain size caused by the formation of a sub-grain structure. In the second region of microhardness there is essentially a stabilization with further increase in the numbers of HPT turn. This observed stabilization is the consequence of a steady state due to the equilibrium between dislocation accumulation and their annihilation caused by dynamic recovery [36, 37].

In order to determine the hardening mechanism in the alloy processed by HPT, the microhardeness values of the HPT-deformed samples at 25 and 250 °C were plotted against the grains size as shown in Fig. 8 for the two processing temperatures. It is obvious for both deformation conditions that the microhardness increases with decreasing grain size.

These values can be fitted linearly by the Hall-Petch relationship that describes the grain-boundary hardening through the relationship:

$$H_v = H_{v0} + kd^{-1/2} \quad (2)$$

where *Hv* is the microhardness at the corresponding grain size *d*, Hv_0 is the microhardeness intercept at $d^{-1/2} = 0$ and *k* is the Hall-Petch slope. The values of Hv_0 and *k* for both deformation temperatures are presented in Fig. 8. The slope of the Hall-Petch curve after HPT processing at 25 °C is slightly larger than for the alloy processed by HPT at 250 °C.

These results are in good agreement with other data for the Hall–Petch relationship for ultrafine-grained (100–1000 nm) materials produced by SPD processing [38, 39]. In nanostructured alloys below ~10 nm an inverse Hall-Petch relationship may occur due mainly to the operation of grain boundary sliding [40] but a deviation from the Hall–Petch relationship was also reported at grain sizes smaller than ~ 500 nm in an Al–Mg–Si alloy processed by HPT at room temperature [21] and this was explained by the easy movement of extrinsic dislocations in the non-equilibrium grain boundaries introduced by HPT processing. Finally, it should be noted that these deviations from the Hall-Petch relationship differ from the deviation that occurs when processing by HPT to very low strains, typically through 1/4 to 1 turn, where the deviation is due to the large fraction of grain boundaries having low angles of misorientation [41].

Very recently, an enhanced hardness was reported in nanocrystalline Fe-Ni alloys [42] which exhibit smaller grain size but lower hardness (~240 in Vickers hardness) in comparison with the ~380 hardness achieved in the present HPT samples. Nanocrystalline FeNi alloys with grain sizes ranging from 40 to 70 nm were prepared by compaction under 172, 682, and 1194 MPa and sintered at 600-900 °C in hydrogen. These authors observed that the hardness of the alloys prepared at 800 and 900 °C was lower than that of the alloy prepared at 700 °C and the samples sintered at 600 °C and 1194 MPa exhibited the highest hardness of 242.2 Hv. They assumed that the relationship between the hardness and the preparation conditions is rather complex Moreover, the annealing time should be another important factor for the final grain size and density. The samples sintered at 600 °C and 1194 MPa exhibited the highest hardness of 242.2 Hv. The effect of oxides on the hardness must also be considered [42].

Finally, it is obvious that the microhardness is dependent on not only the grain size, but also on the processing method. It is worth noting that extremely larger strains are introduced during HPT processing than compaction and sintering. The dominant microstructural features that are nanoscale/ultrafine grains and extremely high densities of GBs are often quantified by the mean grain size *d* [43**]**. There are special structural features that are sensitive to material characteristics and the synthesis/processing history. Examples of the special features include grain shapes, grain size distribution, dominant types and structures of GBs, single-phase/composite structure, second-phase geometry, fabrication-induced flaws, nano-twins, and compositional inhomogeneity [43].

A special emphasis has to be placed on the importance of HAGBs in systems produced by SPD processing that have particular non-equilibrium structures [43]. Such non-equilibrium structures are characterized by a diffuse appearance in TEM micrographs due to their excess grain boundary energy, the presence of long range elastic stresses and enhanced free volumes. They were shown to cause anomalous phenomena such as enhanced lattice diffusion and subsequent structural phase transitions/ ordering reactions as well as dynamic-aging [13, 15, 43]. The Mossbauer spectroscopy method has been used and gave direct information about the atomic redistribution on the level of the nearest atomic neighborhood. It was found that GBs and near-boundary regions in UFG W produced by SPD are characterized by an excess free volume which confirms their non-equilibrium state [44].

5. Conclusions

An Fe-36%Ni (wt.%) alloy with initial grain size of ~8.2 μm and initial Cube {001}<100> texture was processed using HPT up to 10 turns at either ambient temperature or 250 °C. Based on the experimental results, the following conclusions are drawn:

1. A significant grain refinement occurs during HPT processing leading to similar grain sizes of ~ 0.30 and ~ 0.24 μm at ambient temperature and 250 °C, respectively. This similarity occurs because 250 °C is far below the effective temperature for recrystallization and grain growth. A temperature of 250 °C for HPT processing has a weak effect on the microstructure evolution in the alloy.
2. The fraction of HAGBs gradually increases with increasing numbers of HPT turns and saturates after 5 turns. It is slightly higher after processing at 250 °C due the rate of annihilation of dislocations and LAGBs.

3. The crystallographic texture after HPT processing at ambient temperature is characterized by typical A and B fibers of a simple shear FCC texture with a dominant *B* component. By contrast, the *A*, *B* and *C* components develop during HPT processing at 250 °C with *C* as the dominant texture component. This texture difference is associated with the occurrence of dynamic recovery during processing at 250 °C and this is confirmed by the tendency towards texture randomization with increasing numbers of HPT turns.
4. The microhardness increases significantly after 1/2 HPT turn and appears to reasonably saturate after 5 turns. For both HPT processing conditions, there is agreement with a Hall-Petch grain size dependence for the microhardness.

Acknowledgements

The authors wish to thank Pierre-Louis REYDET from APERAM-alloys Imphy Society, France, for kindly providing the Fe-36%Ni alloy. This work was supported in part by the international PHC-MAGHEB program No. 16MAG03. Two of the authors were supported by the European Research Council under ERC Grant Agreement No. 267464-SPDMETALS (YH and TGL).

References

[1] R.Z. Valiev, T.G. Langdon, Principles of equal-channel angular pressing as a processing tool for grain refinement. Prog. Mater. Sci. 51 (2006) 881–981. DOI: https://doi.org/10.1016/j.pmatsci.2006.02.003

[2] Y. Saito, N. Tsuji, H. Utsunomiya, T. Sakai, R.G. Hong. Ultra-fine grained bulk aluminum produced by accumulative roll-bonding (ARB) process. Scripta Mater. 39, (1998) 1221–1227. DOI: https://doi.org/10.1016/S1359-6462(98)00302-9

[3] A.P. Zhilyaev, T.G. Langdon, Using high-pressure torsion for metal processing: Fundamentals and applications. Prog. Mater. Sci. 53 (2008) 893–979. DOI: https://doi.org/10.1016/j.pmatsci.2008.03.002

[4] X. Sauvage, G. Wilde, S. Divinsky, Z. Horita, R.Z. Valiev. Grain boundaries in ultrafine grained materials processed by severe plastic deformation and related phenomena. Mater. Sci. Eng. A 540 (2012) 1–12. DOI:10.1016/j.msea.2012.01.080

[5] R.Z. Valiev, M. Zehetbauer, Y. Estrin, H.W. Höppel, Y. Ivanisenko, H. Hahn, G. Wilde, H.J. Roven, X. Sauvage, T.G. Langdon, The Innovation Potential of Bulk Nanostructured Materials, Adv. Eng. Mater. 9 (2007) 527–533. DOI: https://doi.org/10.1002/adem.200700078

[6] M.J. Zehetbauer and Y.T. Zhu, Bulk Nanostructured Materials, Wiley-VCH, Weinheim, Germany, 2009.

[7] A. Y. Khereddine, F. Hadj Larbi, H. Azzeddine, T. Baudin, F. Brisset, A.L. Helbert, M.H. Mathon, M. Kawasaki, D. Bradai, T. G. Langdon. Microstructures and textures of a Cu–Ni–Si alloy processed by high-pressure torsion. J. Alloys Compd. 574 (2013) 361–367. DOI: https://doi.org/10.1016/j.jallcom.2013.05.051

[8] J. Wongsa-Ngam, M. Kawasaki, T.G. Langdon. A comparison of microstructures and mechanical properties in a Cu-Zr alloy processed using different SPD techniques. J. Mater. Sci. 48 (2013) 4653–4660. DOI: https://doi.org/10.1007/s10853-012-7072-0

[9] L. Mishnaevsky, E. Levashov, R. Z. Valiev, J. Segurado, I. Sabirov, N. Enikeev, S. Prokoshkin, A. V. Solov'yov, A. Korotitskiy, E. Gutmanas, I. Gotman, E. Rabkin, S. Psakh'e, L. Dluhos , M. Seefeldt , A. Smolin. Nanostructured titanium-based materials for medical implants: Modeling and development. Mater. Sci. Eng. R 81 (2014) 1–19. DOI: https://doi.org/10.1016/j.mser.2014.04.002

[10] K. Tirsatine, H. Azzeddine, T. Baudin, A-L Helbert, F. Brisset, B. Alili, D. Bradai. Texture and microstructure evolution of Fe-Ni alloy after accumulative roll bonding. J. Alloys Compd. 610 (2014) 352–360. DOI: https://doi.org/10.1016/j.jallcom.2014.04.173

[11] H. Azzeddine, K. Tirsatine, T. Baudin, A-L. Helbert, F. Brisset, D. Bradai. Texture evolution of Fe-Ni alloy sheet produced by cross accumulative roll bonding. Mater. Charact. 97 (2014) 140–149. DOI: https://doi.org/10.1016/j.matchar.2014.09.009

[12] B.L. Li, N. Tsuji, N. Kamikawa. Microstructure homogeneity in various metallic materials heavily deformed by accumulative roll-bonding. Mater. Sci. Eng. A 423 (2006) 331–342. DOI: https://doi.org/10.1016/j.matchar.2014.09.009

[13] S. Lee, K. Edalati, H. Iwaoka , Z. Horita , T. Ohtsuki , T. Ohkochi , M. Kotsugi , T. Kojima, M. Mizuguchi, K. Takanashi. Formation of FeNi with $L1_0$-ordered structure using high-pressure torsion. Philos. Mag. Lett. 94 (2014) 639–646. DOI: https://doi.org/10.1080/09500839.2014.955546

[14] L. Y. Pustov, V.V. Tcherdyntsev, S.D. Kaloshkin, E.I. Estrin, E.V. Shelekhov, A.I. Laptev, D.V. Gunderov. Face-centered cubic phase stability and martensitic transformation under deformation in Fe–Ni and Fe–Mn alloys nanostructured by mechanical alloying and high-pressure torsion. Mater Sci. Eng. A 481–482 (2008) 732–736. DOI: https://doi.org/10.1016/j.msea.2006.12.203

[15] T. Ohtsuki, M. Kotsugi, T. Ohkochi, S. Lee, Z. Horita, K. Takanashi. Nanoscale characterization of FeNi alloys processed by high-pressure torsion using photoelectron

emission microscope. J. Appl. Phys. 114(2013) 143905. DOI: https://doi.org/10.1063/1.4824372

[16] S. Lee, Z. Horita. Annealing Behavior of FeNi alloy processed by high-pressure torsion. Mater. Sci. Forum 667-669 (2011) 313–318. DOI: 10.4028/www.scientific.net/MSF.667-669.313

[17] R.B. Figueiredo, P.H.R. Pereira, M.T.P. Aguilar, P.R. Cetlin, T.G. Langdon. Using finite element modeling to examine the temperature distribution in quasi-constrained high-pressure torsion. Acta Mater. 60 (2012) 3190–3198. DOI: https://doi.org/10.1016/j.actamat.2012.02.027

[18] F. Bachmann, R. Hielscher, H. Schaeben. Texture analysis with MTEX – Free and open source software toolbox. Solid State. Phenom. 160 (2010) 63–68. DOI: 10.4028/www.scientific.net/SSP.160.63

[19] I.J. Beyerlein, L. S. Tóth. Texture evolution in equal-channel angular extrusion. Prog. Mater. Sci. 54 (2009) 427–510. DOI: https://doi.org/10.1016/j.pmatsci.2009.01.001

[20] L.S. Tóth, J.J. Jonas, D. Daniel, J.A. Bailey. Texture development and length changes in copper bars subjected to free end torsion. Textures Microstruct. 19 (1992) 245–262. DOI: http://dx.doi.org/10.1155/TSM.19.245

[21] A. Loucif, R. B. Figueiredo, T. Baudin, F. Brisset, R. Chemam, T. G. Langdon. Ultrafine grains and the Hall–Petch relationship in an Al–Mg–Si alloy processed by high-pressure torsion. Mater. Sci. Eng. A 532 (2012) 139–145. DOI: https://doi.org/10.1016/j.msea.2011.10.074

[22] S.V. Dobatkin, S.V. Shagalina, O.I. Sleptsov, N.A. Krasil'nikov. Effect of the initial state of a low-carbon steel on nanostructure formation during high-pressure torsion at high strains and pressures. Rus. Metall. (Metally) 2006 2006 445–52. DOI: https://doi.org/10.1134/S0036029506050120

[23] G.G. Maier, E.G Astafurova, V.S. Koshovkina, G.V. Chomyakova, E.V. Naydenkin, P.D. Odessky, S.V. Dobatkin. The influence of temperature on microstructure and microhardness in high-pressure torsion of low-carboon steel. IOP Conf. Series: Mater. Sci. Eng. 63 (2014) 012133. DOI:10.1088/1757-899X/63/1/012133

[24] Y. Huang, R. B. Figueiredo, T. G. Langdon. Effect of HPT processing temperature on strength of a Mg-Al-Zn alloy. Rev. Adv. Mater. Sci. 31 (2012) 129–137.

[25] F.J. Humphreys, M. Hatherly, Recrystallization and related annealing phenomena, second ed., Elsevier, Oxford, UK, 2004. p. 192.

[26] P.W. Bridgman. Flow phenomena in heavily stressed metals. J. Appl. Phys. 8 (1937) 328–336.

[27] S. Zaefferer, T. Baudin, R. Penelle. A study on the formation mechanisms of the cube recrystallization texture in cold rolled Fe–36%Ni alloys. Acta Mater. 49 (2001) 1105–1122. DOI: https://doi.org/10.1016/S1359-6454(00)00387-6

[28] K. Tirsatine, H. Azzeddine, T. Baudin, A.L. Helbert, F. Brisset, D. Bradai. On the thermal stability of Fe-36%Ni alloy after accumulative roll bonding and annealing at 600 °C. Materials Engineering 24 (2017) 56–66. DOI: http://fstroj.uniza.sk/journal-mi/PDF/2017/07-2017.pdf

[29] K.S. Suresh, S. Sinha, A. Chaudhary, S. Suwas. Development of microstructure and texture in Copper during warm accumulative roll bonding. Mater. Charact. 70 (2012) 74–82. DOI: https://doi.org/10.1016/j.matchar.2012.04.017

[30] B. Han, Z. Xu. Microstructural evolution of Fe–32%Ni alloy during large strain multi-axial forging. Mater. Sci. Eng. A 447 (2007) 119–124. DOI: https://doi.org/10.1016/j.msea.2006.10.010

[31] M. Kawasaki, Z. Horita, T.G. Langdon. Microstructural evolution in high purity aluminum processed by ECAP. Mater. Sci. Eng. A524 (2009) 143–150. DOI: https://doi.org/10.1016/j.msea.2009.06.032

[32] U.F. Kocks, C.N. Tomé, H.R. Wenk, Texture and Anisotropy: Preferred Orientations in Polycrystals and Their Effect on Materials Properties, Cambridge University Press, 2000.

[33] D. Orlov, P. P. Bhattacharjee, Y. Todaka, M. Umemoto, N. Tsuji. Texture evolution in pure aluminum subjected to monotonous and reversal straining in high-pressure torsion. Scripta Mater. 60 (2009) 893–896. DOI: https://doi.org/10.1016/j.scriptamat.2009.02.004

[34] A. Loucif, Y. Huang, A.L. Helbert, T. Baudin, S. Sabbaghianrad, T. G. Langdon. Microtextural changes and superplasticity in an Al-7075 alloy processed by high-pressure torsion. Mater. Sci. Forum 838-839 (2016) 445–450. DOI: 10.4028/www.scientific.net/MSF.838-839.445

[35] K. Edalati, Z. Horita. Significance of homologous temperature in softening behavior and grain size of pure metals processed by high-pressure torsion. Mater. Sci. Eng. A 528 (2011) 7514–7523. DOI: https://doi.org/10.1016/j.msea.2011.06.080

[36] K. Edalati, T. Fujioka, Z. Horita. Microstructure and mechanical properties of pure Cu processed by high-pressure torsion. Mater. Sci. Eng. A 497 (2008) 168–173. DOI: https://doi.org/10.1016/j.msea.2008.06.039

[37] M. Kawasaki. Different models of hardness evolution in ultrafine-grained metals processed by high-pressure torsion. J. Mater. Sci. 49 (2014) 18–34. DOI: https://doi.org/10.1016/j.jmrt.2014.06.002

[38] R.Z. Valiev. Superior strength in ultrafine-grained materials produced by SPD processing. Mater. Trans. 55 (2014) 13–18. DOI: https://doi.org/10.2320/matertrans.MA201325

[39] N. Balasubramanian, T.G. Langdon, The strength-grain size relationship in ultrafine-grained metals, Metall. Mater. Trans. A 47A (2016) 5827–5838. DOI https://doi.org/10.1007/s11661-016-3499-2

[40] M.A. Meyers, A. Mishra, D.J. Benson. Mechanical properties of nanocrystalline materials. Prog. Mater. Sci. 51 (2006) 427–556. DOI: https://doi.org/10.1016/j.pmatsci.2005.08.003

[41] P. Bazarnik, Y. Huang, M. Lewandowska, T.G. Langdon. Structural impact on the Hall-Petch relationship in an Al-5Mg alloy processed by high-pressure torsion. Mater. Sci. Eng. A 626 (2015) 9–15. DOI: https://doi.org/10.1016/j.msea.2014.12.027

[42] P.Z. Si, C. J. Choi. High hardness nanocrystalline Invar alloys prepared from Fe-Ni nanoparticles. Metals 8 (2018) 28–36. DOI: doi:10.3390/met8010028

[43] I.A. Ovid'ko, R.Z. Valiev, Y.T. Zhu, Review on superior strength and enhanced ductility of metallic nanomaterials, Prog. Mater. Sci. 94 (2018) 462-540. doi: https://doi.org/10.1016/j.pmatsci.2018.02.002

[44] V.V. Popov, A V. Stolbovsky, A.V. Sergeev, V.A. Semionkin, Mössbauer spectroscopy of grain boundaries in ultrafine-grained materials produced by severe plastic deformation. Bull. Russian Acad. Sci.: Physics 81 (2017) 860–864. DOI
https://doi.org/10.3103/S106287381707022X

Figures and Table Caption

Figure 1: IPF maps showing the microstructures of Fe-36%Ni (wt.%) alloy after HPT at ambient temperature through: a) 1/2, b) 1, c) 5 and d) 10 turns.

Figure 2: IPF maps showing the microstructures of Fe-36%Ni (wt.%) alloy after HPT at 250 °C through: a) 1/2, b) 1, c) 5 and d) 10 turns.

Figure 3: Evolution of the mean grain size and HAGB with number of HPT turn of Fe-36%Ni (wt.%) alloy after HPT at ambient temperature and 250 °C.

Figure 4: ODF sections at φ_2= 45° obtained from EBSD measurements of Fe-36%Ni (wt.%) alloy after HPT processing for 1/2 to 10 turns at ambient temperature and 250 °C, respectively.

Figure 5: Volume fraction of shear texture components versus number of HPT turns at: a) ambient temperature and b) 250 °C.

Figure 6: Evolution of microhardness of Fe-36%Ni (wt.%) alloy after HPT processing up 10 turns at ambient temperature and 250 °C, respectively.

Figure 7: Evolution of the texture index value of Fe-36%Ni (wt.%) alloy after HPT processing up 10 turns at ambient temperature and 250 °C, respectively.

Figure 8: Evolution of microhardness as a function of the grain size after HPT processing at: (a) ambient temperature and (b) 250 °C through 1/2, 1, 5 and 10 turns.

Table 1. Ideal HPT orientations for FCC materials.

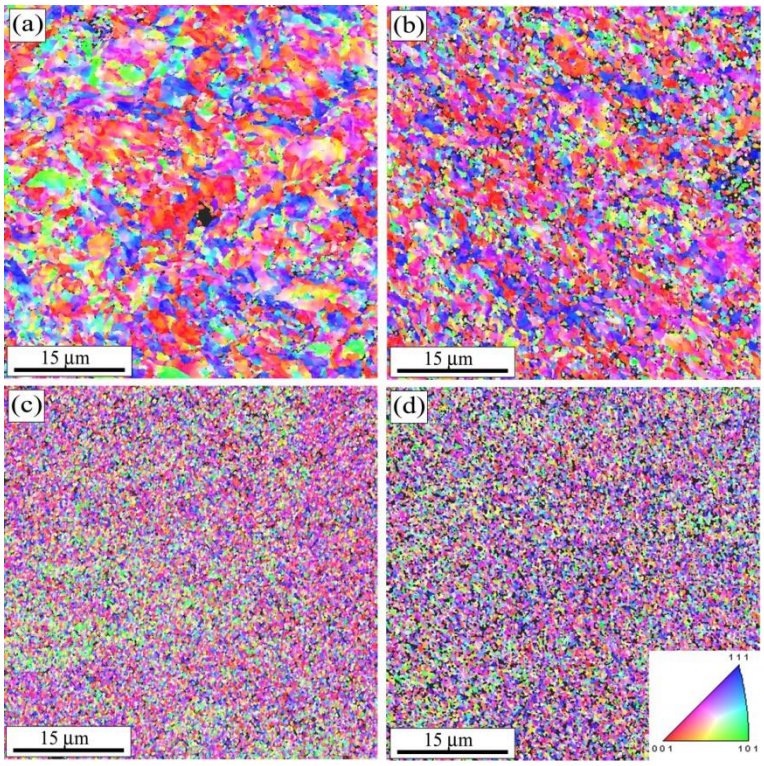

Figure 1: IPF maps showing the microstructures of Fe-36%Ni (wt.%) alloy after HPT at ambient temperature through: a) 1/2, b) 1, c) 5 and d) 10 turns.

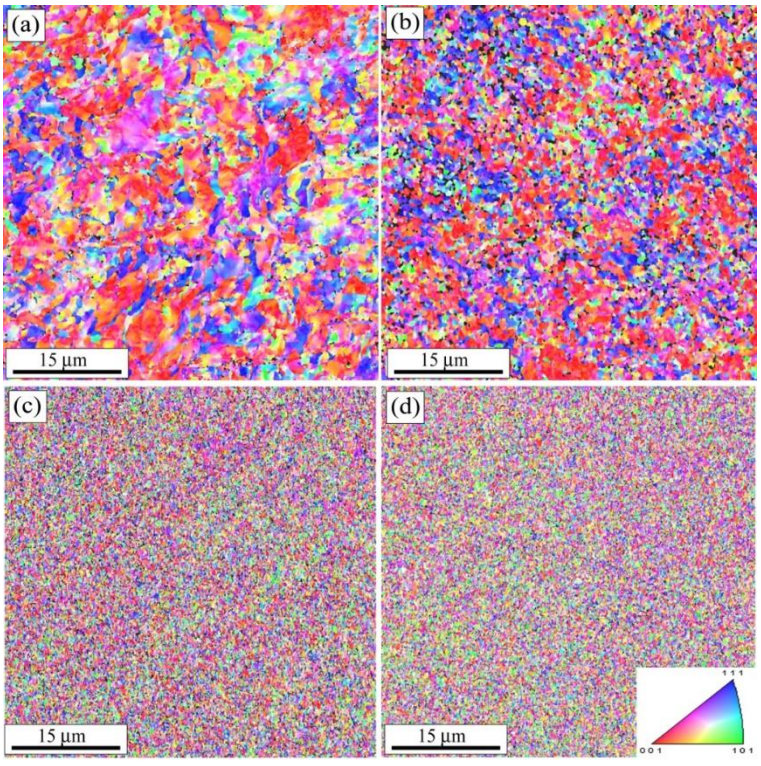

Figure 2: IPF maps showing the microstructures of Fe-36%Ni (wt.%) alloy after HPT at 250 °C through: a) 1/2, b) 1, c) 5 and d) 10 turns.

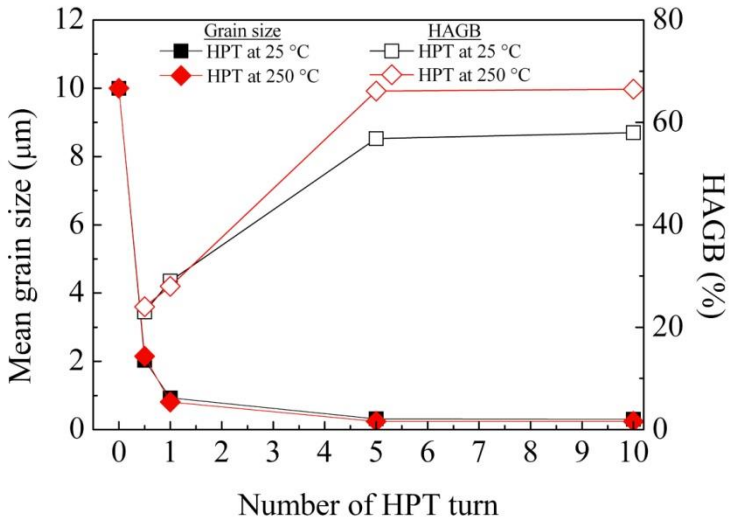

Figure 3: Evolution of the mean grain size and HAGB with number of HPT turn of Fe-36%Ni (wt.%) alloy after HPT at ambient temperature and 250 °C.

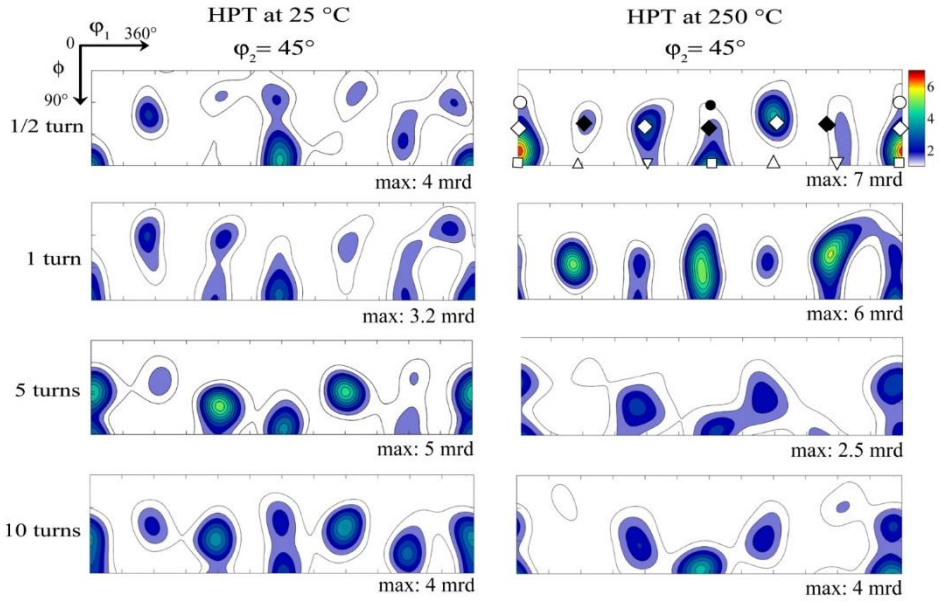

Figure 4: ODF sections at φ_2= 45° obtained from EBSD measurements of Fe-36%Ni (wt.%) alloy after HPT processing for 1/2 to 10 turns at ambient temperature and 250 °C.

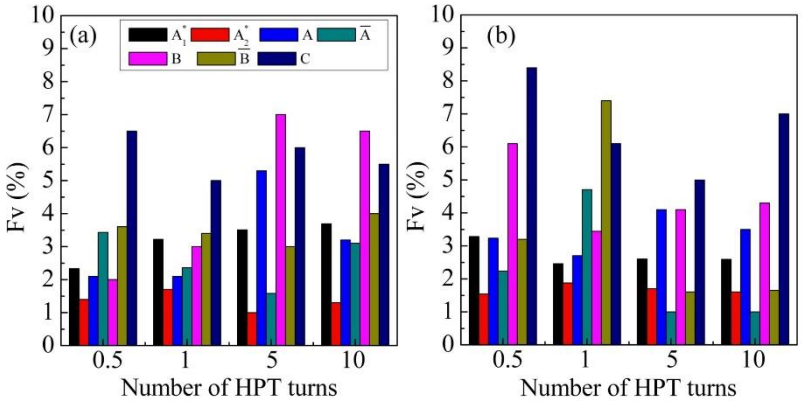

Figure 5: Volume fraction of shear texture components versus number of HPT turns at: a) ambient temperature and b) 250 °C.

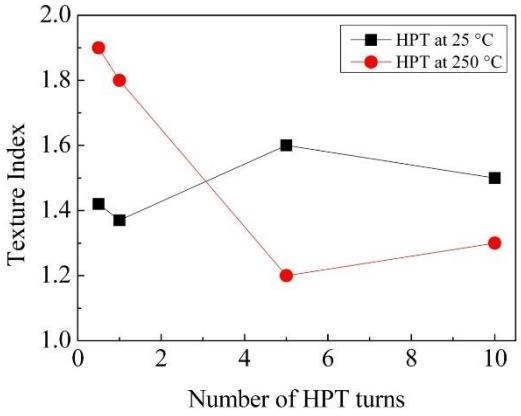

Figure 6: Evolution of the texture index value of Fe-36%Ni (wt.%) alloy after HPT processing up 10 turns at ambient temperature and 250 °C, respectively.

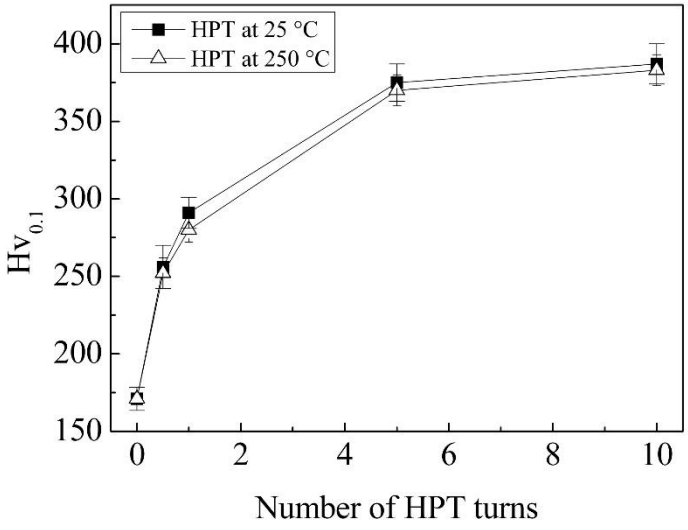

Figure 7: Evolution of microhardness of Fe-36%Ni (wt.%) alloy after HPT processing up 10 turns at ambient temperature and 250 °C, respectively.

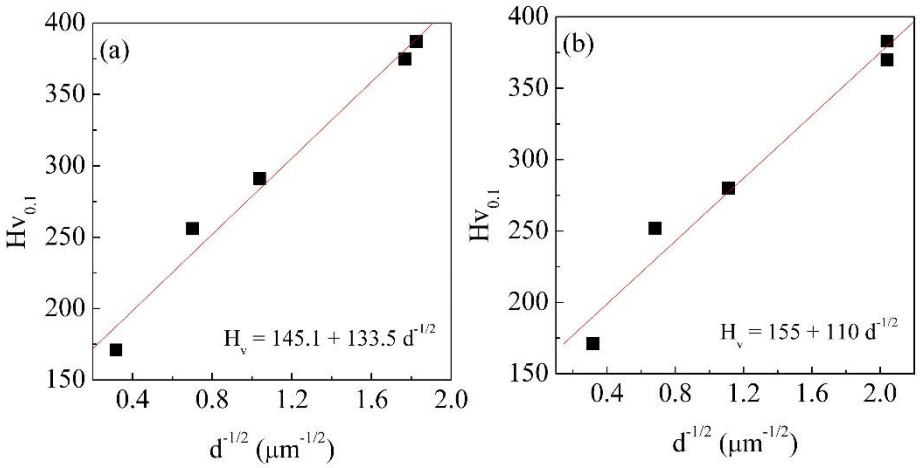

Figure 8: Evolution of microhardness as a function of the grain size after HPT processing at: (a) ambient temperature and (b) 250 °C through 1/2, 1, 5 and 10 turns.

Table 1. Ideal HPT orientations for FCC materials.

Component	**Euler Angle**		
	φ_1	ϕ	φ_2
A_1^* ▽	125.26/305.26°	90°	45°
A_2^* △	54.7/234.7°	90°	45°
A ○	0°	35.26°	45°
$\overline{A}$ ●	180°	35.26°	45°
B ◇	0/120/240°	54.74°	45°
$\overline{B}$ ◆	60/180/300°	54.74°	45°
C □	0/180°	90°	45°